Microbubble generation in a co-flow device operated in a new regime

Elena Castro-Hernández,[a] Wim van Hoeve,[b] Detlef Lohse,[b] and José M. Gordillo*[a]

Received Xth XXXXXXXXXX 20XX, Accepted Xth XXXXXXXXX 20XX
First published on the web Xth XXXXXXXXXX 200X
DOI: 10.1039/b000000x

A new regime of operation of PDMS-based flow-focusing microfluidic devices is presented. We show that monodisperse microbubbles with diameters below one-tenth of the channel width (here $w = 50\,\mu$m) can be produced in low viscosity liquids thanks to a strong pressure gradient in the entrance region of the channel. In this new regime bubbles are generated at the tip of a long and stable gas ligament whose diameter, which can be varied by tuning appropriately the gas and liquid flow rates, is substantially smaller than the channel width. Through this procedure the volume of the bubbles formed at the tip of the gas ligament can be varied by more than two orders of magnitude. The experimental results for the bubble diameter d_b as function of the control parameters are accounted for by a scaling theory, which predicts $d_\mathrm{b}/w \propto (\mu_\mathrm{g}/\mu_\ell)^{1/12}\left(Q_\mathrm{g}/Q_\ell\right)^{5/12}$, where μ_g and μ_ℓ indicate, respectively, the gas and liquid viscosities and Q_g and Q_ℓ are the gas and liquid flow rates. As a particularly important application of our results we produce monodisperse bubbles with the appropriate diameter for therapeutical applications ($d_\mathrm{b} \simeq 5\,\mu$m) and a production rate exceeding 10^5 Hz.

Introduction

Microbubble formation is an area of growing interest due to its countless applications in food processing,[1] material science,[2] pharmacy and medicine.[3] In the last decades, microbubbles have become the most effective type of contrast agent available for medical ultrasound imaging[4–6] or as carriers for targeted drug delivery.[7,8] In order to ensure that microbubbles can safely flow through the smallest capillaries, the diameter of the microbubbles injected into the patient's blood stream needs to be between 1 and $10\,\mu$m; the preferred diameter is between $2\,\mu$m and $5\,\mu$m. Larger bubbles may provoke edema and smaller ones possess a poor reflectivity.

Microbubbles with sizes in the correct range for therapeutical purposes can be easily produced by either sonication or by mechanical agitation.[9–12] The generation of bubbles with a size below $1\,\mu m$ can be achieved through the injection of a gas using porous membranes, which requires an extremely high working pressure typically of the order of 10 MPa.[13] However, all these procedures generate a polydisperse emulsion of bubbles in the liquid, limiting the potential use of microbubbles in medicine. Indeed, it is of current interest for therapeutical applications to design a simple procedure for the mass production of microbubbles with controllable diameters ranging from 2 to $5\,\mu$m and *with a low polydispersity index,* typically PDI$= s/r_b < 5\times10^{-2}$, with r_b the averaged bubble radius and s the standard deviation.[3] When the values of the PDI are sufficiently low (say, below 5%), the bubbles are considered as monodisperse. Perfect monodispersity PDI$= 0$ can obviously never be achievable. Note that the monodispersity is essential when microbubbles are used as ultrasound contrast agents to improve the quality of an echographical image. In the case that microbubbles are used as drug carriers, very low values of the PDI index are also demanded in order to precisely control the amount of the drug delivered into the patient.

In this manuscript we will describe and characterize in detail a novel process for the production of the type of microbubbles needed for therapeutical applications. More specifically, we propose a novel method for the production of $\simeq 5\,\mu$m bubbles with a PDI of 5% and better and at a production rate that exceeds 10^5 Hz.

Probably, the simplest way of producing monodisperse bubbles is to inject a small gas flow rate through an underwater nozzle.[14,15] Unfortunately, the bubbles released from a needle with a diameter of 5 microns into a stagnant reservoir of water is $\sim 50\,\mu m$, *much larger* than the injection needle diameter. Clearly, this method is not feasible for the production of monodisperse bubbles with potential therapeutical applications. However, it is known from the early works of Bragg and Nie[16] –who modeled the dynamic structure of crystals through a wet foam composed of monodisperse bubbles[17]– that bubbles with sizes comparable to the needle diameter can be generated when a small amount of gas is injected within a liquid crossflow[16] or a liquid coflow.[18] Since then, it has been shown that micron-sized bubbles can be produced if a suffi-

[a]*Área de Mecánica de Fluidos, Departamento de Ingeniería Aeroespacial y Mecánica de Fluidos. Universidad de Sevilla. Avda. de los Descubrimientos s/n, 41092, Sevilla, Spain. Fax: +34 954486041; Tel: +34 954481185; E-mail: jgordill@us.es*
[b]*Physics of Fluids, Faculty of Science and Technology, University of Twente, P.O. Box 217, 7500 AE Enschede, The Netherlands.*

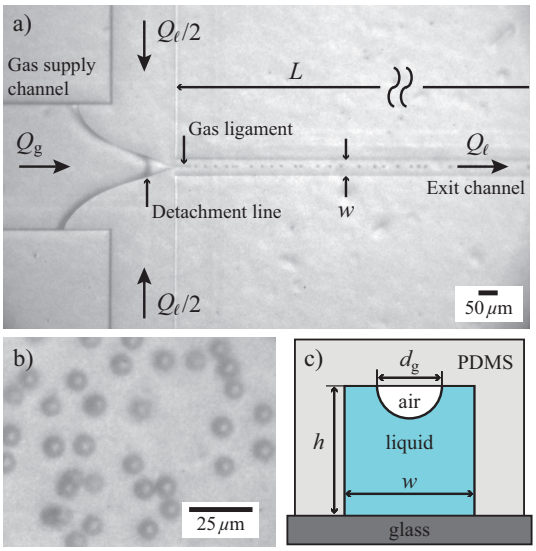

Fig. 1 (a) High speed photograph showing the formation of microbubbles using our microfluidic flow-focusing geometry, $w = 50\,\mu$m, $L/w = 30$. The outer liquid flow forces the inner gas flow to form a tiny gas ligament that detaches from the channel wall and breaks up into microbubbles. The size of the microbubbles $d_b = 7.2\,\mu$m is much smaller than the channel width. The gas and liquid pressures are $p_g = 1555$ mbar and $p_\ell = 1597$ mbar, respectively, and the liquid flow rate is $U_\ell = 7.67\,\mathrm{m\,s^{-1}}$. (b) Microbubbles immediately after exiting the channel. (c) Schematic representation of a cross-section of the microfluidic channel downstream the detachment line. The gaseous ligament dewets the PDMS channel wall.

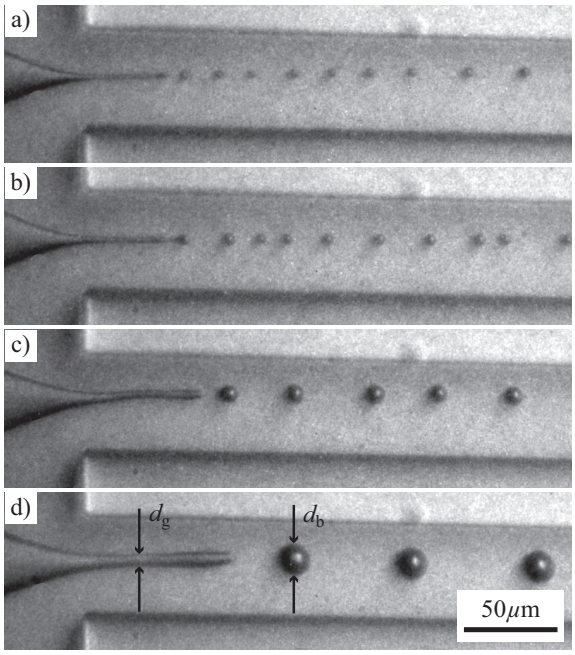

Fig. 2 The size of the microbubbles produced can be accurately varied by adapting the gas and liquid flow rates by controlling their driving pressures. In order for $Q_g/Q_\ell \ll 1$, the gas pressure in the supplying vessel, p_g, is chosen to be very similar to that of the liquid, p_l. The operating conditions corresponding to each of the four images are: a) $p_\ell = 1800$ mbar, $p_g = 1757$ mbar, $U = 8.67\,\mathrm{m\,s^{-1}}$, $d_b = 4.33\,\mu$m, $d_g = 2.60\,\mu$m; b) $p_\ell = 1800$ mbar, $p_g = 1763$ mbar, $U = 8.67\,\mathrm{m\,s^{-1}}$, $d_b = 5.73\,\mu$m, $d_g = 2.92\,\mu$m; c) $p_\ell = 1410$ mbar, $p_g = 1383$ mbar, $U = 6.83\,\mathrm{m\,s^{-1}}$, $Q_g = 0.0044\,\mathrm{ml\,min^{-1}}$, $d_b = 10.05\,\mu$m, $d_g = 3.90\,\mu$m; d) $p_\ell = 1410$ mbar, $p_g = 1463$ mbar, $U = 6.83\,\mathrm{m\,s^{-1}}$, $Q_g = 0.0134\,\mathrm{ml\,min^{-1}}$, $d_b = 15.58\,\mu$m, $d_g = 5.84\,\mu$m. From this figure note that, as expected, for a fixed value of Q_ℓ (or p_ℓ), d_b increases as p_g increases.

ciently small tube or channel through which a gas is injected, is placed in a strong liquid coflow[14,19–25] or crossflow.[26–33] Usually, the liquid is forced to flow thanks to an imposed pressure gradient. Farook *et al.* and Pancholi *et al.*[34–36] implemented the coaxial electrospray configuration described by Loscertales *et al.*[37] to generate 5 μm bubbles. In this particular case, the liquid coflow is induced by the electrical tangential stresses. However, this production technique does not result in the formation of microbubbles with a sufficiently narrow size distribution.

An alternative way for the production of virtually monodisperse microbubbles at high and controlled production rates is to use a procedure called flow-focusing.[38–41] Here, a strong coflow of liquid is created when both the liquid and gas streams are forced to flow through a small constriction. Placing a cylindrical gas injection tube in front of an orifice of smaller diameter, Gañán and Gordillo[42] produced bubbles with $d_b \sim O(10)\,\mu$m, which are typically *smaller* than the orifice diameter, by simply controlling the flow rate ratio. Indeed, the diameter d_b of the bubbles obtained in this way is given, approximately, by $d_b \propto (Q_g/Q_\ell)^\beta$, with $\beta \simeq 0.38 \simeq 2/5$, $Q_g/Q_\ell < 1$ and with Q_g and Q_ℓ indicating the gas and liquid flow rates, respectively.[42,43]

However, due to the fact that the alignment of the injection tube with the exit orifice is not an easy task, the parallelization of this type of axisymmetric devices for the mass production of microbubbles is not straightforward. Later on, Anna *et al.*,[44] Gordillo *et al.*[45] and Garstecki *et al.*[46] circumvented this limitation of axisymmetric flow focusing bubble makers by implementing the same geometry in planar devices. Planar microfluidic devices built using soft lithography techniques and incorporating the flow focusing geometry, are nowadays used by many research groups to produce monodisperse bubbles with therapeutical purposes.[47–50]

We stress that, though the flow focusing geometry in the planar version[46] is very similar to the axisymmetric one,[42] the physical mechanism leading to bubble formation is sub-

stantially different in both types of devices. For the axisymmetric case,[42] liquid velocities are such that the dimensionless groups *We* and *Re* satisfy $We \gg 1$ and $Re \gg 1$. Note that the Weber number *We* quantifies the relative importance of surface tension stresses with respect to liquid inertia and is defined as $We = \rho U^2 w/\sigma$, with ρ, U and σ indicating the liquid density, the liquid mean velocity and surface tension coefficient respectively and w the transversal dimension of the exit channel. On the other hand, the dimensionless group that compares viscous stresses with respect to liquid inertia is the Reynolds number, defined as $Re = \rho U w/\mu_\ell$, with μ_ℓ the liquid viscosity. Due to the fact that $We \gg 1$ and $Re \gg 1$, bubble formation in the experiments reported by Gañán and Gordillo[42] is controlled by liquid inertia. However, the typical liquid flow rates injected in the planar version of flow focusing are so small (10^{-2} to 1 μL s^{-1}), that $We \ll 1$ and $Re \lesssim 1$ and, in addition, the capillary numbers ($Ca = \mu_\ell U/\sigma$) are typically such that ($Ca < 10^{-2}$).[46,51,52] Therefore, liquid inertia is negligible when compared to viscous shear stresses and viscous shear is not strong enough to overcome capillary pressure.[31] Under these conditions, bubbles block almost the whole cross section of the exit channel, forcing the carrier fluid to flow through thin wetting films straddling at the walls of the device. This fact results in a significant increase of the liquid pressure upstream of the emerging bubble, leading to the 'squeezing' of the gas thread.[31] Except in the final stage of the collapse, in which gas inertia accelerates the bubble pinch-off process,[53,54] the mechanism of bubble formation is mainly controlled by the gas and liquid flow rates and by the device geometry.

A direct consequence of the geometrically controlled mechanism of bubble formation is that the polydispersity index of the bubbles generated through the 'squeezing' mechanism is below 5%; moreover, Garstecki *et al.* found that the bubble size can be expressed as a function of the ratio of gas and liquid flow rates as $d_b \propto (Q_g/Q_\ell)^{1/3}$. Note that the exponent $1/3$, which differs from the exponent $\simeq 2/5$ that characterize bubble size in the axisymmetric flow focusing devices, already reflects the differences in the way bubbles are formed in both types of geometries. But there is an even more important difference between the two types of implementations: since bubbles block the exit channel in the planar version of flow focusing, the diameters of the bubbles formed in this way are necessarily larger than the width of the exit channel. Contrarily, in the axisymmetric version of flow focusing devices, d_b is smaller than the exit orifice diameter as pointed out above.

This fact has an important consequence when bubbles are produced using the planar flow focusing geometry, namely, bubbles with sizes of the order of 5 μm obviously require the use of tiny microchannels of widths $w \approx 5\,\mu$m (see *e.g.* Hettiarachchi *et al.*[47]). We implemented the flow focusing geometry incorporating exit channels of widths of 5 μm and experienced that these tiny channels tend to clog very easily due to the accumulation of impurities. Thus, we decided to find a different way for the production of 5 micron bubbles that differs from the methods already existing in the literature.[46–51,53]

Here we describe a new method for the controlled production of $\sim 5\,\mu$m bubbles with a polydispersity index below 5 % at high production rates ($> 10^5$ bubbles/s) by means of a planar flow focusing device. The essential geometrical difference of our device with respect to *all* previous implementations is that the length of the exit channel L is much larger than its width, namely, $L/w \gg 1$, as depicted in figure 1. This, together with the fact that the imposed liquid and gas flow rates are such that $Re \gtrsim 10^2$, $We \gg 1$ and $Q_g/Q_\ell \ll 1$, enables the production of bubbles in water with sizes one order of magnitude smaller than the channel width. In this way, we are able to produce, in a single step, bubbles with sizes within the range needed for therapeutical applications avoiding clogging problems. The final result, which we present in detail in the "Results" section and derive in the "Discussion" section, is that bubble size can be predicted based on the gas to liquid flow rate ratio and the fluid properties as

$$d_b/w \simeq 2.75(\mu_g/\mu_\ell)^{1/12}(Q_g/Q_\ell)^{5/12}. \qquad (1)$$

Equation (1) is applicable *if* the gas and liquid flow rates satisfy the conditions $Q_g/Q_\ell \ll 1$ and

$$\frac{Q_\ell}{Q_0} > 3\left(\frac{Q_g}{Q_0}\right)^{-1/7}, \qquad (2)$$

where the reference flow rate Q_0 is given by

$$Q_0 = \left(\frac{\sigma w^3}{\rho}\right)^{1/2}. \qquad (3)$$

Note that the exponent $5/12$ in equation (1), which differs from the exponents $1/3$ and $2/5$ to calculate bubble diameter as a function of the ratio Q_g/Q_l reported in previous publications[42,46], reveals that our method is different from those already published. The differences can be visually appreciated in figure 2: in our device, bubbles are formed after the formation of a long gas jet, whose diameter is much smaller than the channel width, and bubbles breakup up from its tip. The gas jet, which has a diameter of only a few microns, is formed at the entrance of the exit channel, where the liquid pressure gradient reaches its maximum value. To our knowledge, this is the first time that the existence of such tiny and stable gas jets within a microchannel is described. Note, however, that Anna *et al*[44] report experimental evidence of the formation of very thin liquid threads, similar to those appreciated in figure 2, but in the case of the focused fluid is a liquid instead of a gas. Moreover, this is the first time that bubbles with a size of one-tenth the channel width are produced in a low viscosity liquid

such as water. Since a long gas jet is created before bubbles are emitted from its tip, bubbles are not formed in the way described in Ref.[42]. Clearly, since bubbles do not block the exit channel, they are not produced in the 'squeezing' regime described by Garstecki *et al.*[31,46,51] either. Let us point out that the advantage of microbubble formation in the way presented in this paper as compared to the *squeezing* regime is that bubbles with sizes in the range of interest for medical applications ($d_b \lesssim 5\,\mu$m) at frequencies that exceed 10^5 Hz are formed from a square microchannel of $50 \times 50\,\mu$m^2 cross sectional area. This one order of magnitude reduction in bubble size with respect to channel width, avoids the clogging of the exit channel and enormously decreases the pressures at which both the gas and the liquid need to be injected into the microfluidic device. Our procedure also allows to easily vary the bubble volume over more than two orders of magnitude by simply varying the gas and liquid flow rates.

The paper is organized as follows: in section 'Materials and methods', we describe in detail the experimental procedure followed to generate micron-sized bubbles. In section 'Results' we report the bubble formation frequencies as well as their associated PDI as a function of bubble diameter. In addition, we indicate the ranges of both the gas and liquid flow rates needed to create bubbles of less than 10 microns. For those readers interested in technical details, equations (1) and conditions (2)-(3) are deduced in section 'Discussion'. The final section of the paper is dedicated to present the conclusions of our study.

Materials and methods

The bubble generators were produced by soft lithography techniques. A mold was created from a negative photosensitive material (SU-8 GM 1060, Gersteltec SARL) and spin-coated on a silicon oxide substrate, to imprint a reticulable polymer PDMS (Polydimethylsiloxane), Sylgard 184, Dow Corning) which was irreversibly bounded to a glass cover plate in a plasma cleaner. We placed the microbubble-generating devices in an oven at 65° during one hour and they were used only after 24 hours to ensure the hydrophobicity of the PDMS. Note that, contrarily to most microfluidic applications, we impose the hydrophobicity of the PDMS[52] since, in our case, the gas ligament should remain attached to the PDMS surface for stability purposes. The height of the microbubble maker is uniform and equal to $h = 50\,\mu$m and the width and length of the exit channel are, respectively, $w = 50\,\mu$m and $L = 1500\,\mu$m (see Fig. 1). Note that the main geometrical difference between our bubble generator and those used in previous studies[46,47,51,53] is that, in order for bubbles to be formed at the entrance region of the exit channel, our devices satisfy the condition $L/w \gg 1$. To avoid fluctuations in the gas flow rate, air was injected through a tube with 0.5 m in length and $50\,\mu$m of inner diameter. The air pressure, p_g, was controlled through a pressure regulator (Bosch Rexroth) and was measured using a digital manometer (Digitron 2000P). The continuous phase was distilled water with a $2\%\,(w/v)$ of Tween 80 (Sigma Aldrich) added. The addition of the surfactant lowered the water-air interfacial tension coefficient to $\sigma \simeq 40$ mN/m and the contact angles with the PDMS and glass substrates were, respectively, $\theta_{PDMS} = 89°$ and $\theta_{glass} = 39.5°$. Since the liquid was supplied from a pressurized vessel instead of from a syringe pump, the liquid injection pressure, p_ℓ, was controlled and measured in the same way as the gas. The liquid flow rate Q_ℓ was determined by measuring the volume of liquid collected at the exit of the device during several minutes. The setup was placed under an inverted microscope (3000B Leica) which was connected to either a high-speed camera (Phantom V 7.3, with a resolution of 80×16 pixels and a field of view of $163 \times 33\,\mu$m^2 when operated at an acquisition rate of 2×10^5 fps) or to an Intensified Retiga Fast camera (resolution of 1280×800 pixels, with a field of view of $415 \times 260\,\mu$m^2). We checked the perfect reproducibility of the experiments. To take data, experiments were repeated twice for each couple of values p_ℓ, p_g: First, the bubbling frequency ω was determined using the high-speed camera. Second, in an independent experiment for the same parameters the bubble diameter d_b was measured from the high-resolution images taken with the intensified camera. Knowing ω and d_b, the volumetric gas flow rate was determined as $Q_g = \pi d_b^3 \omega/6$. We checked that the values of Q_g calculated in this way were practically identical – albeit more accurate – to those obtained assuming Poiseuille flow along the gas injection pipe.

Results

Figure 1 shows a global view of the microchannel entrance region, which is where the microbubbles are formed. The figure reveals that – thanks to our choice $Q_g/Q_\ell < 0.03$ – the gas filament contracts from the width of the gas supply channel ($400\,\mu$m) to a steady ligament whose diameter is substantially smaller than w. Due to the fact that the height (h) of the device is equal to the width of the exit channel ($h = w \gg d_b$), the gas thread separates from the lower glass surface at the region indicated as *detachment line* in Fig. 1. Indeed, since the PDMS substrate is less hydrophilic than the glass one ($\theta_{PDMS} \simeq 90°$ and $\theta_{glass} = 39.5°$), the narrow gas ligament, of diameter $d_g \ll w$, is attached to the upper PDMS surface, as sketched in Fig. 1c. Once the steady gas ligament is formed, it breaks into uniformly sized bubbles with diameters $d_b \sim d_g$, as depicted in Fig. 2. In figures 3a-b we plot, as a function of d_b, the bubbling frequencies extracted from the analysis of the high speed videos and their corresponding values of the PDI calculated from the image analysis of the high resolution pictures. Clearly, figures 3a-b reveal that our procedure enables

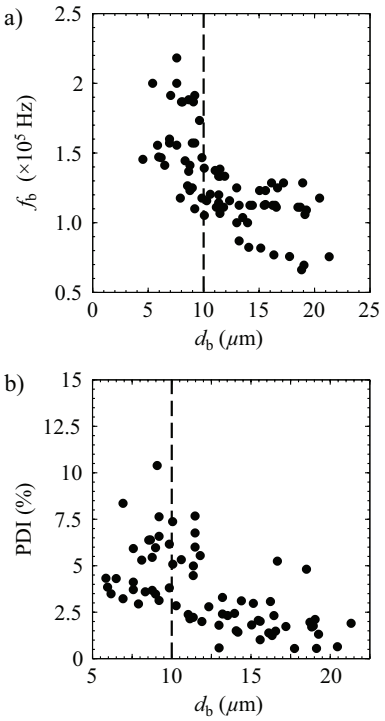

Fig. 3 (a) Bubble formation frequencies as a function of bubble diameter. Note that all bubbles with diameters below 10 μm are produced at frequencies that exceed 10^5 Hz. (b) PDI index, in %, as a function of bubble diameter. Note that for many experimental conditions bubbles with diameters $d_b \simeq 5\,\mu$m can be produced with values of the PDI index below 5%. The reason for which the (apparent) PDI index is larger for some experiments is attributable to the fact that some images are out of the focus plane and are a bit blurred.

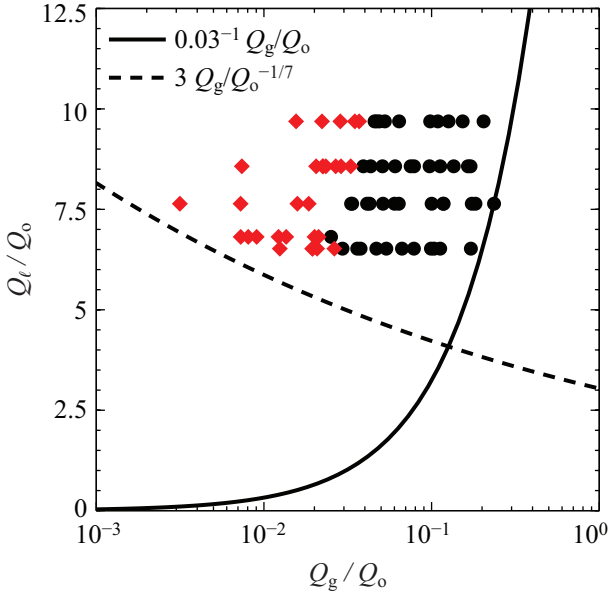

Fig. 4 Values of the liquid and gas flow rates considered in this study. Liquid velocities were varied between 6 m s^{-1} and 8.5 m s^{-1} , whereas the gas flow rate varied between 4×10^{-4} ml min^{-1} and 4×10^{-2} ml min^{-1}. Red diamonds indicate the operating conditions for which $d_b < 10\,\mu$m whereas black dots indicate $d_b > 10\,\mu$m. Note that the liquid and gas flow rates considered here satisfy the condition $Q_g/Q_\ell \ll 1$ as well as the condition $Q_\ell/Q_0 > 3(Q_g/Q_\ell)^{-1/7}$ given in equation (2). This latter condition is deduced from the fact that, in order for the gas ligament to be formed, the Weber number based on the gas ligament diameter namely, $We_j = \rho U^2 d_g/\sigma$ (see figure 2 for a definition of d_g), needs to be above a certain constant or order unity.

the production of bubbles with diameters $\simeq 5\,\mu$m and very low polydispersity index at frequencies that exceed 10^5 *Hz*.

We will now indicate the range of values of Q_ℓ and Q_g for which bubbles with sizes substantially smaller than the channel width, are produced. Note first that the mean liquid velocity along the exit channel, $U = Q_\ell/(w^2)$, needs to be above a certain threshold. Indeed, the liquid pressure decreases by an amount of $\Delta p_\ell \simeq \rho U^2$ from the detachment line to the inlet of the exit channel. Since the liquid pressure drop is much larger than the gas pressure variation in the same region, namely, $\Delta p_g \sim \mu_g Q_g/w^3$, the normal stress condition at the gas-liquid interface, when evaluated at the channel inlet can be expressed as $\rho U^2 \simeq 2\sigma/d_g$, implying $\mathrm{We}_j = \rho U^2 d_g/\sigma > \mathrm{We}_{\min} \simeq 2.5$. If d_g is expressed as a function of the ratio Q_g/Q_ℓ by means of equation (5) – deduced in the beginning of the next section – it is straightforward to show that the condition $\mathrm{We}_j > 2.5$ is equivalent to the one given by equation (2), which expresses that the liquid flow rate has to be above a certain threshold that depends on the gas flow rate. Moreover, in order to generate bubbles with sizes substantially smaller than the channel width, we also choose to impose the condition $Q_g/Q_\ell \leq 0.03$ i.e, the liquid flow rate has to be substantially larger than the gas one. Clearly, as depicted in figure 4, the different experiments considered in this study satisfy the conditions $Q_g/Q_\ell \ll 1$ and that given in equation (2). The data points represented with red diamonds indicate those experimental conditions for which bubbles with diameters below 10 μm are produced, which are of particular interest for their use as ultrasound contrast agents.

Discussion of the results

Scaling of the gas ligament diameter

Note first that, for the range of liquid velocities investigated here, $\mathrm{Re} = U d_b/\nu_\ell \sim O(10^2)$ with $\nu_\ell \simeq 10^{-6}\,m^2\,s^{-1}$ the kinematic viscosity of water. This estimate indicates that the flow in the exit channel is laminar. Moreover, for the range of

Reynolds numbers considered here, the entrance length is such that $L_e \simeq 0.1 Q_\ell/\nu_\ell \simeq 1.5L$. Therefore, since the gas ligament breaks at a distance of $\sim h \ll L_e$ from the duct inlet (see Fig. 2), bubbles are produced within the entrance region of the microchannel. In this entrance region, the liquid velocity profile is approximately uniform except at the thin boundary layers of typical width $\delta \ll w$ near the walls.[55]

Moreover, since the gas Reynolds number is such that $\mathrm{Re_g} = Q_g/(\nu_g d_b) \sim O(1)$, being ν_g the kinematic viscosity of air, the flow rate along the gas ligament can be calculated as

$$Q_g = -K \frac{d_g^4}{\mu_g} \frac{\mathrm{d}p_g}{\mathrm{d}x}, \qquad (4)$$

where μ_g is the gas viscosity, K is a constant and $\mathrm{d}p_g/\mathrm{d}x$ indicates the pressure gradient along the gas jet. Due to the fact that the cross-section of the ligament hardly varies downstream (*cf.* Fig. 2), $-\mathrm{d}p_g/\mathrm{d}x$ approximately coincides with the liquid pressure gradient evaluated at the channel inlet, $-\mathrm{d}p_\ell/\mathrm{d}x = C\mu_\ell U/w^2$, with μ_ℓ the liquid viscosity and C is a constant that depends on the geometry of the channel and on the width δ of the liquid boundary layers at the channel walls. Note that the smaller δ, the larger C and therefore the liquid pressure gradient is maximal at the duct entrance.[55] For instance, in the particular case of a circular channel with a fully developed Poiseuille flow, for which $\delta \simeq w$, the pressure gradient is given by $-d\,p_g/d\,x = 32\mu_\ell U/w^2$. Consequently, since $\delta \ll w$, the constant C satisfies $C \gg 32$.[55] Now, as expressed by equation (4), d_g decreases for a fixed value of Q_g when $-d\,p_g/d\,x = -d\,p_\ell/d\,x = C\mu_\ell U/w^2$ increases. We conclude that, thanks to the large values of C – i.e., thanks to the fact that bubbles are produced at the duct entrance – d_g can be reduced down to only a few microns, as depicted in figure 2. With $-d\,p_g/d\,x = C\mu_\ell U/w^2$ equation (4) yields the following expression for d_g:

$$\frac{d_g}{w} \propto \left(\frac{\mu_g}{\mu_\ell}\right)^{1/4} \lambda^{1/4}, \qquad (5)$$

where $\lambda = Q_g/Q_\ell$. Fig. 5 shows that the best fit to the experimental data follows very closely the prediction $d_g \propto \lambda^{1/4}$ of equation 5, validating our physical reasoning.

Bubble size

We now must only find the size of the bubbles as a function of d_g, U, and Q_g. First, note from Fig. 2 that the gas ligament breaks only slightly downstream the channel inlet. At this location, the liquid pressure gradient is smaller than $C\mu_\ell U/w^2$ and thus, according to equation (4), d_g must increase in order to keep Q_g constant. Indeed, this is seen in Fig. 2. The increase in the jet diameter triggers the bubble formation process and also induces variations in the gas pressure gradient of

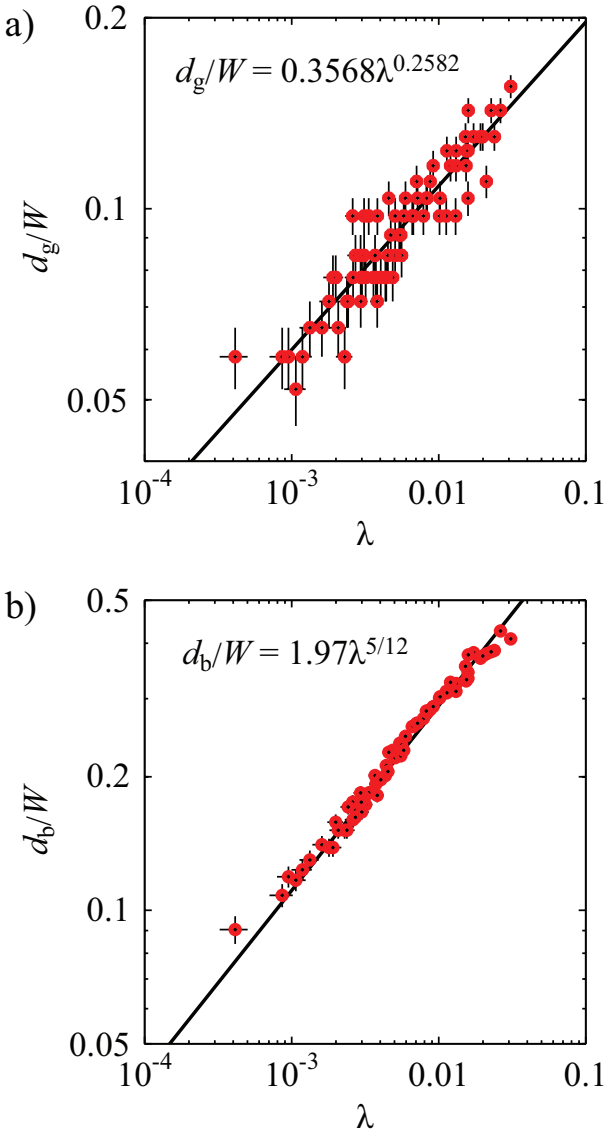

Fig. 5 (a) Optically measured (minimal) width d_g of the gas ligament as function of the gas flow ratio λ. In spite of the large error bars associated to the fact that d_g is of the order of only a few microns, the best fit to the experimental data (straight line) closely follows the prediction $\propto \lambda^{1/4}$ given by equation 4. (b) Optically measured microbubble diameter d_b as function of the gas flow ratio, together with the scaling law $d_b/w \propto \lambda^{5/12}$ following from the presented scaling theory. Here the error bars are smaller as the bubbles are spherical and larger than the minimal width of the gas ligament.

the order of $\Delta(\mathrm{d}p_\mathrm{g}/\mathrm{d}x) \sim \sigma/(d_\mathrm{g}\, w)$.* Thus, since $C \gg 32$,[55] the relative variation of the gas flow rate is given by

$$\frac{\Delta Q_\mathrm{g}}{Q_\mathrm{g}} = \frac{\Delta(\mathrm{d}p_\mathrm{g}/\mathrm{d}x)}{\mathrm{d}p_\mathrm{g}/\mathrm{d}x} \sim \frac{1}{C}\frac{\sigma}{\mu_\ell U}\frac{w}{d_\mathrm{g}} \ll 1\,. \qquad (6)$$

The condition expressed by equation (6) means that bubbles are formed under constant flow rate conditions[21] and, consequently, the bubbling frequency is given by $\omega \propto U/d_\mathrm{g}$.[14,21,42] Therefore, the bubble diameter can be easily calculated from the mass balance as

$$\frac{\pi d_\mathrm{b}^3}{6} \propto Q_\mathrm{g}\frac{d_\mathrm{g}}{U} \rightarrow \frac{d_\mathrm{b}}{w} \propto \left(\frac{\mu_\mathrm{g}}{\mu_\ell}\right)^{1/12}\lambda^{5/12}. \qquad (7)$$

Figure 5b shows that once the proportionality constant is fixed to 2.75, equation (7) predicts the size of the bubbles formed with a maximum relative error of $\pm 10\%$. This maximum relative error corresponds to the minimum value of λ. We attribute this small discrepancy between experiments and theory to the fact that, for the smallest values of d_g, the gas ligament is embedded within the liquid boundary layer, resulting into a smaller local liquid velocity and thus an underestimation of λ.

Conclusions and Outlook

To conclude, we succeeded to produce monodisperse microbubbles in a controllable and reproducible way with microchannels with dimensions of tens of microns, avoiding clogging problems, and easily being able to adjust the microbubble size by varying the liquid and gas flow rates. We have provided the operating conditions in terms of the gas and liquid flow rates for which microbubbles with $d_\mathrm{b} < 10\,\mu$m and, thus, in the size range required for medical applications, can be produced with very low values of the PDI index at frequencies that exceed 10^5 Hz. From the point of view of applications, our method is able to produce $\sim 10^{10}$ virtually monodisperse microbubbles with $d_\mathrm{b} \simeq 5\,\mu$m with a total energy consumption of only ~ 200 J.

Moreover, we could theoretically account for this new regime of operation of the coflow device: The central issues are an extremely low gas flow rate (as compared to the liquid flow rate) and a strong pressure gradient in the entrance region of the channel where the microbubbles form. The theory allows to derive the correct scaling laws for the microbubble size as function of the control parameters.

The next step will be to stabilize the formed bubbles by phospholipids or surfactants to prevent that the bubbles dissolve or coalesce in the pool where they are trapped. If one succeeds, the new device allows for an alternative way to produce ultrasound contrast agents, with presumably a much sharper distribution of bubble sizes, *i.e.*, monodisperse bubbles. For commercial applications one obviously has to go beyond PDMS devices (*e.g.*, silicon), to guarantee stable long time behavior. Another issue is the mass production for real applications, but the fact that our devices incorporate the flow focusing region in a planar geometry, facilitates the multiplexation of these types of devices.[56] Anyway, typically, the number of bubbles injected into a patient's blood stream is $\sim 10^{10}$ bubbles. Since this is the amount of bubbles generated by just one device during one day, one hundred of these devices working in parallel would create 100 doses a day with a power consumption of only $\sim 1\,W$.

* In this estimate it has been taken into account that the length of the gas ligament is $\simeq w$ (*cf.* Fig. 2)

Acknowledgments

We would like to thank Lingling Shui, Hao Gu, and David Fernandez Rivas for technical assistance in the fabrication of the microfluidic devices. We kindly acknowledge Michel Versluis and Benjamin Dollet for discussions. The UTwente part of the present work was financially supported by the MicroNed technology program of the Dutch Ministry of Economic Affairs through its agency SenterNovem under grant Bsik-03029.5. E.d.C. and J.M.G. thank the financial support by both the Spanish Ministry of Education under project DPI2008-06624-C03-01 and the Junta de Andalucía under project P08-TEP-03997.

References

1 R. Zúñiga and J. Aguilera, *Trends Food Sci. Tech.*, 2008, **19**, 176–187.
2 K. S. Suslick and G. J. Price, *Ann. Rev. Mat. Sci.*, 1999, **29**, 295–326.
3 E. Stride and M. Edirisinghe, *Soft Matter*, 2008, **4**, 2350–2359.
4 E. Stride and R. Tang, M-X. Eckersley, *Appl. Acoust.*, 2009, **70**, 1352–1362.
5 S. M. van der Meer, B. Dollet, M. M. Voormolen, C. T. Chin, A. Bouakaz, N. de Jong, M. Versluis and D. Lohse, *J. Acoust. Soc. Am.*, 2007, **121**, 648–656.
6 J. R. Lindner, J. Song, F. Xu, A. L. Klibanov, K. Singbartl, K. Ley and S. Kaul, *Circulation*, 2000, **102**, 2745–2750.
7 K. Ferrara, M. Borden and H. Zhang, *Acc. Chem. Res.*, 2009, **42**, 881–892.
8 K. Ferrara, R. Pollard and M. Borden, *Ann. Rev. Biomed. Eng.*, 2007, **9**, 415–447.
9 Y. Z. Zhao, H. D. Liang, X. G. Mei and M. Halliwell, *Ultrasound Med. Biol.*, 2005, **31**, 1237–1243.
10 W. Nyborg, *Ultrasound Med. Biol.*, 2001, **27**, 301–333.
11 B. B. Jiang, C. Y. Gao and J. C. Shen, *Colloid Polym. Sci.*, 2006, **284**, 513–519.
12 C. Christiansen, H. Kryvi, P. Sontum and T. Skotland, *Biotechnol. Appl. Biochem.*, 1994, **19**, 307–320.
13 M. Kukizaki and M. Goto, *J. Membr. Sci*, 2006, **281**, 386–396.
14 H. N. Oğuz and A. Prosperetti, *J. Fluid Mech.*, 1993, **257**, 111–145.
15 R. Bolaños, A. Sevilla, C. Martínez-Bazán and J. M. Gordillo, *Phys.Fluids*, 2008, **20**, 112104.
16 W. L. Bragg and J. F. Nie, *Proc. Roy. Soc. A*, 1947, **190**, 474–481.

17 A. Net, W. Drenckhan, D. Weaire and S. Hutzler, *Soft Matter*, 2006, **2**, 129–134.
18 C. S. Smith, *Jour. Appl. Phys.*, 1949, **20**, 631.
19 S. C. Chuang and V. W. Goldschmidt, *ASME J. Basic Eng.*, 1970, **92**, 705–711.
20 A. Sevilla, J. M. Gordillo and C. Martínez-Bazán, *J. Fluid Mech.*, 2005, **530**, 181–195.
21 J. M. Gordillo, A. Sevilla and C. Martínez-Bazán, *Phys. Fluids*, 2007, **19**, 077102.
22 R. Suryo and O. Basaran, *Phys. Fluids*, 2006, **18**, 082102.
23 A. Utada, A. Fernández-Nieves, H. Stone and D. Weitz, *Phys. Rev. Lett.*, 2007, **99**, 094502.
24 P. Guillot, A. Colin, A. S. Utada and A. Adjari, *Phys. Rev. Lett.*, 2007, **99**, 104502.
25 A. G. Marin, F. Campo-Cortés and J. M. Gordillo, *Colloids Surf. A: Physicochem. Eng. Aspects*, 2009, **344**, 2–7.
26 S. E. Forrester and C. D. Rielly, *Chem. Eng. Sci.*, 1998, **53**, 1517–1527.
27 T. Thorsen, R. W. Roberts, F. H. Arnold and S. R. Quake, *Phys. Rev. Lett.*, 2001, **86**, 4163–4166.
28 J. H. Xu, S. W. Li, Y. J. Wang and G. S. Luo, *Appl. Phys. Lett.*, 2006, **88**, 133506.
29 K. P. Pancholi, E. Stride and M. J. Edirisinghe, *Langmuir*, 2008, **24**, 4388–4393.
30 P. Guillot and A. Colin, *Phys. Rev. E*, 2005, **72**, 066301.
31 P. Garstecki, M. J. Fuerstman, H. A. Stone and G. M. Whitesides, *Lab Chip*, 2006, **6**, 437–446.
32 V. Steijn, C. R. Kleijn and M. T. Kreutzer, *Phys. Rev. Lett.*, 2009, **103**, 214501.
33 V. Steijn, C. R. Kleijn and M. T. Kreutzer, *Lab Chip*, 2010, **10**, 2513–2518.
34 U. Farook, E. Stride and M. Edirisinghe, *J. R. Soc. Interface*, 2009, **6**, 271–277.
35 K. P. Pancholi, U. Farook, E. Stride and M. J. Edirisinghe, *Eur. Biophys. J.*, 2008, **37**, 515–520.
36 U. Farook, E. Stride and M. J. Edirisinghe, *Eur. Biophys. J.*, 2009, **38**, 713–718.
37 I. G. Loscertales, A. Barrero, I. Guerrero, R. Cortijo, M. Marquez and A. Ganan-Calvo, *Science*, 2002, **295**, 1695–1698.
38 O. A. Basaran, *AIChE J.*, 2002, **48**, 1842–1848.
39 A. Gunther and K. Jensen, *Lab Chip*, 2006, **6**, 1487–1503.
40 A. Barrero and I. G. Loscertales, *Annu. Rev. Fluid Mech.*, 2007, **39**, 89–106.
41 C. J. Martinez, *Bubble Science, Engineering and Technology*, 2009, **1**, 40–52.
42 A. Gañán-Calvo and J. M. Gordillo, *Phys. Rev. Lett.*, 2001, **87**, 274501.
43 A. Gañán-Calvo, *Phys. Rev. E*, 2004, **69**, 027301.
44 S. L. Anna, N. Bontoux and H. A. Stone, *Appl. Phys. Lett.*, 2003, **82**, 364–366.
45 J. M. Gordillo, Z. Cheng, M. Márquez, A. Gañán-Calvo and D. Weitz, *Phys. Fluids*, 2004, **16**, 2828–2834.
46 P. Garstecki, I. Gitlin, W. DiLuzio, G. M. Whitesides, E. Kumacheva and H. A. Stone, *Appl. Phys. Lett.*, 2004, **85**, 1487–1503.
47 K. Hettiarachchi, E. Talu, M. Longo, P. Dayton and A. Lee, *Lab Chip*, 2007, **7**, 463–468.
48 E. Talu, K. Hettiarachchi, R. Powell, A. Lee, P. Dayton and M. Longo, *Langmuir*, 2008, **24**, 1745–1749.
49 J. I. Park, Z. Nie, A. Kumachev and E. Kumacheva, *Soft Matter*, 2010, **6**, 630–634.
50 J. I. Park, E. Tumarkin and E. Kumacheva, *Macromol. Rapid Commun.*, 2010, **31**, 222–227.
51 P. Garstecki, H. A. Stone and G. M. Whitesides, *Phys. Rev. Lett.*, 2005, **94**, 164501.
52 P. Tabeling, *Lab Chip*, 2009, **9**, 2428–2436.
53 B. Dollet, W. van Hoeve, J. P. Raven, P. Marmottant and M. Versluis, *Phys. Rev. Lett.*, 2008, **100**, 034504.
54 J. M. Gordillo, A. Sevilla, J. Rodríguez-Rodríguez and C. Martínez-Bazán, *Phys. Rev. Lett.*, 2005, **95**, 194501.
55 L. Rosenhead, *Laminar boundary layers*, Dover Publications, New York, 1988.
56 I. Kobayashi, T. Takano, R. Maeda, Y. Wada, K. Uemura and M. Nakajima, *Microfluid. Nanofluid.*, 2008, **4**, 167–177.